

Article

Stress Distribution on the Preliminary Structural Design of the CENTEC-TLP under Still Water and Wave-Induced Loads

Esmaeil Zavvar , Hossam S. Abdelwahab , Emre Uzunoglu , Bai-Qiao Chen  and C. Guedes Soares * 

Centre for Marine Technology and Ocean Engineering (CENTEC), Instituto Superior Técnico,
Universidade de Lisboa, 1049-001 Lisboa, Portugal

* Correspondence: c.guedes.soares@centec.tecnico.ulisboa.pt

Abstract: An assessment is made of the stress distribution and the hydrodynamic response of the preliminary structural design of the tension leg platform of a 10 MW wind turbine. The platform supporting a 10 MW turbine is modelled and analysed by the finite element method. The stress distribution of the platform is determined in still water with the turbine at above-rated conditions, and the response of the tension leg platform is estimated in the time domain. The results of the time domain analysis show reasonable agreement between the present results and the available data. To check the design stiffener dimensions, span, and spacing against stress distribution, classification societies' recommendations are used. The results of the stress distribution analysis indicate that the critical locations of the platform are the interaction of the lower columns with the upper columns and the connection of the tower of the turbine.

Keywords: still water; CENTEC tension leg platform (CENTEC-TLP); hydrodynamic response; finite element models; time domain



Citation: Zavvar, E.; Abdelwahab, H.S.; Uzunoglu, E.; Chen, B.-Q.; Guedes Soares, C. Stress Distribution on the Preliminary Structural Design of the CENTEC-TLP under Still Water and Wave-Induced Loads. *J. Mar. Sci. Eng.* **2023**, *11*, 951. <https://doi.org/10.3390/jmse11050951>

Academic Editor: Kamal Djidjeli

Received: 21 February 2023

Revised: 13 April 2023

Accepted: 22 April 2023

Published: 28 April 2023



Copyright: © 2023 by the authors. Licensee MDPI, Basel, Switzerland. This article is an open access article distributed under the terms and conditions of the Creative Commons Attribution (CC BY) license (<https://creativecommons.org/licenses/by/4.0/>).

1. Introduction

In response to the ever-increasing need for electrical energy, several research projects have been conducted to identify strategies for the generation of a sizeable amount of power. Consequently, there has been a shift in attention towards the improvement of more environmentally friendly energy sources such as different forms of renewable energy. Wind turbines have received notice as a potential alternative among various other options as the economic prospects for their application are very good [1]. The usage of onshore wind has been prevalent for several decades, but offshore wind farms have been developing at a large pace [2]. Several studies have been made about possible locations for offshore wind farms and about the criteria to rank their economic potential [3]. Different kinds of support structures have been used [4], in particular the spar [5], semisubmersible [6], tension leg platform [7], and barge type [8]. Several of the present studies are being made for turbines of 10 MW, using as the reference model the one specified in [9].

Some researchers investigated the stress distribution on offshore wind turbines and support structures. For example, Reyno et al. [10] did research on the stress concentration in the door opening under design loading conditions. According to the results, the average value of the stress concentration is 1.45, while the amount of reduction achieved by reinforcement was 78%. Umut et al. [11] studied the effects that gravity, rotor forces, and wind loads/vortex loads have on the behaviour of square cross-sections of wind turbine towers with varying wall thicknesses. It was determined that square cross-sections might be a workable alternative to the more commonly used circular cross-sections.

Within the offshore wind turbines, there are two different categories of supporting structures which are fixed bottom and floating structures, both of which are subject to fatigue. For instance, Yeter et al. [12] investigated a fixed offshore wind turbine support structure subjected to combined wave and wind-induced loading. It was concluded that the brace component experienced the most severe fatigue damage, and the estimated fatigue

life was above 1000 years. Yeter et al. [13] designed a jacket offshore wind turbine support structure installed in water depths of 40, 60, and 80 m. The final dimensions were verified by free vibration, structural strength, and stability assessments.

Regarding floating turbines, there are also studies investigating the different types of platforms. Teixeira et al. [14] performed a fatigue analysis for the tower of offshore wind turbines. Kim et al. [15] investigated a support structure of a floating wind turbine to evaluate the effect of wind speed on the stress transfer function. To this end, an artificial neural network (ANN) was used to minimize the number of simulations while increasing the accuracy of the findings. To increase the accuracy of the ANN model, a superposition model was developed. In another study on floating turbines, Bachynski and Moan [16] performed a study on the design and dynamic analysis of a single-column 5 MW tension leg platform wind turbine (TLPWT). It was concluded that for some TLPWTs, second-order sum-frequency wave forces are important for fatigue and extreme response calculations. Ringing forces of third order were shown to be essential for TLPWTs with large diameters (14–18 m), particularly when the turbine was idle or parked.

Oguz et al. [17] performed a numerical and experimental study on a SeaStar-type TLP floating offshore 5 MW wind turbine in regular and irregular waves with wind conditions. It was concluded that the surge, pitch, and heave motion of the experimental and the numerical results have a good agreement, but the roll, sway, and yaw motions were insignificant. A coupled analysis for a floating 5 MW wind turbine, which is fixed by mooring to the bed, was conducted by Sclavounos et al. [18]. The authors indicated that TLPs, due to their low root mean square response have the potential to offer benefits accelerations and negligible heave and pitch motions.

Nematbakhsh et al. [19] compared the typical potential flow calculations of wave-induced loads with CFD calculations demonstrating how detailed analysis can be performed. Jamalkia et al. [20], on the other hand, showed how the analysis of the dynamics response of the structure could be used for detecting damage.

While most of these studies were made with turbines of the order of 5 MW, more recent studies address platforms with 10 MW turbines [21–23].

The design of the tension leg platform which is the main subject of this paper has been used as a reference for the design of a wind farm in the north of Spain [24]. For this area, the environmental conditions have been assessed using specific models to determine the conditions of wind [25], waves [26], and currents [27].

Uzunoglu and Guedes Soares [7,28] explained the design process of the TLP platform and conducted a numerical investigation of the CENTEC-TLP with the 10 MW DTU wind turbine. The results showed minimal wave and wind responses in transport and operational conditions. The frequency domain design solution was conducted with in-house code, and NREL's FAST provided the time-domain solution verification. Tank testing was carried out within the ARCWIND project [29]. In the numerical design study, three environmental conditions consisting of rated, above-rated, and 50-year extreme, was published. The study concluded that the designed model had restrained responses in free-floating conditions, and installed conditions, and the structure of the TLP did not experience any problems regarding mooring breaking, slack, or excessive surge motions. Given the satisfactory dynamic response performance, the preliminary structural design of the CENTEC-TLP has been conducted and this study contributes to the understanding of stress distribution on this 4-column TLP hull.

This work aims to assess the preliminary structural design of the CENTEC-TLP 4-column design against the class society guidelines and to identify the locations exposed to higher stresses. Therefore, the platform is structurally analysed in still water conditions using ANSYS[®] APDL, with wind thrust applied at a constant rated wind speed. Then, hydrodynamic analysis is performed under wave and wind loads. In addition, a comparison with the results of the earlier work of Uzunoglu and Guedes Soares [7] is carried out. Finally, the stress distribution is evaluated on the sections of the platform to identify the critical sections that require further reinforcements.

2. Description of the System and Guidelines

2.1. Description of the Model

In this study, the CENTEC-TLP with the 10 MW DTU wind turbine is analysed to define the stress distribution under hydrostatic pressure. The characteristics of the platform and the wind turbine are presented in Figure 1, Tables 1 and 2. The overall length and breadth of the TLP are 49, while the wind turbine has a total mass (rotor, nacelle, and tower) of 1302 tonnes and a height of 129 m. The total mass of the whole structure (Rotor, Nacelle, Tower, TLP) is 23,388 tonnes. The installed draft is 20 m. Further information on the DTU 10 MW is available in Uzunoglu and Guedes Soares [7], and Bak et al. [9]. The CENTEC-TLP is moored by 12 mooring lines distributed in groups of three mooring lines at each corner. The properties of the mooring lines are shown in Table 3. The mass properties of the tower, turbine, and TLP are shown in Table 4. The properties of the stiffeners are shown in Figure 2 and Table 5. Young’s modulus and Poisson’s ratio are 210 GPa and 0.3, respectively. Steel NV-550 with 550 MPa yield stress is defined in this study.

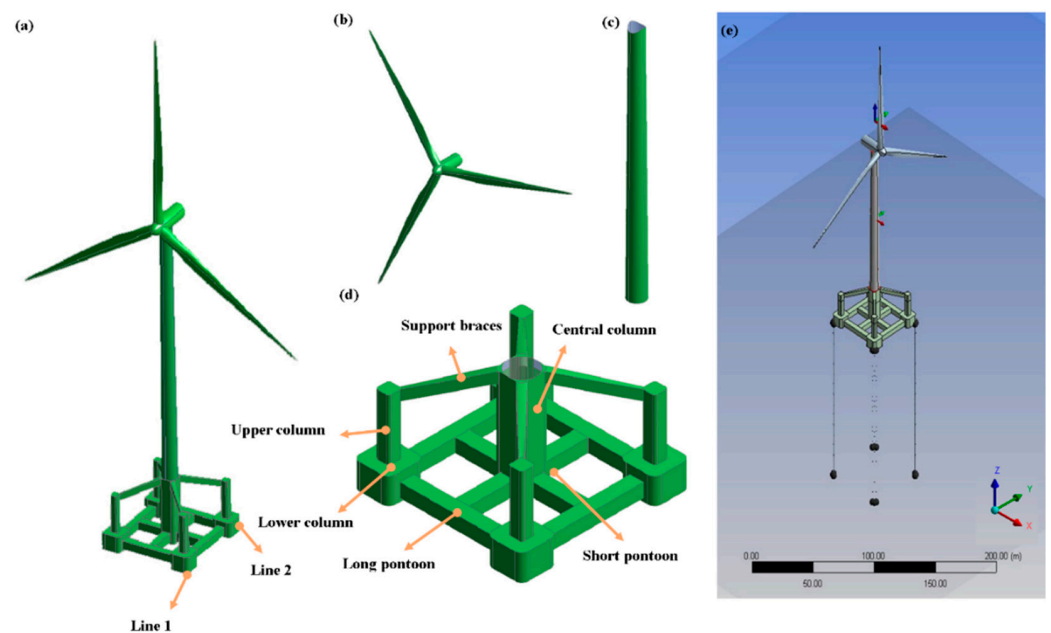


Figure 1. A model of the CENTEC-TLP with the DTU 10 MW. (a) A perspective view of the platform with the turbine in ANSYS APDL; (b) the blades of the wind turbine; (c) the tower; (d) the platform. (e) A perspective view of the platform with the turbine with mooring lines in ANSYS AQWA.

Table 1. Properties of the CENTEC-TLP.

Parameters	Value	Units
Pontoon diameters	4	(m)
Lower column height	7.5	(m)
Lower column diameter	10.5	(m)
Upper column height	17.5	(m)
Upper column side length	4	(m)
Height of the central column above the waterline	10	(m)
Steel thickness of components below installed draft	0.04	(m)
Steel thickness of components above-installed draft	0.04	(m)
Transport draft	3.85	(m)
Transport GM	27.76	(m)
Draft when installed	20	(m)
Volume	3422.4	(m)
Displacement (operational and installed)	3511	(ton)
Steel density	7850	(kg/m)

Table 2. The DTU 10 MW properties Hmedi et al. [29].

Parameter	Value	Units
Cut in wind speed	4	(m/s)
Cut out wind speed	25	(m/s)
Rated wind speed	11.4	(m/s)
Rated power	10	(MW)
Minimum/maximum rotor speeds	6–9.6	(rpm)
Rotor frequency (1P)	6.5–10	(s)
Blade passing frequency (3P)	2.08–3.33	(s)
Number of blades	3	(-)
Rotor diameter	178.3	(m)
Hub diameter	5.6	(m)
Hub height	129	(m)
Rotor mass	227,962	(kg)
Nacelle mass	446,036	(kg)
Tower mass	628,442	(kg)
Total mass of Rotor, Nacelle, Tower	1,302,440	(kg)

Table 3. Mooring line properties [30].

Parameter	Value	Units
Material	6 strand IWRC	(-)
Diameter	14	(cm)
Breaking strength	12,600	(kN)
EA	1.17×10^9	(N)
Number of lines	12	(-)
Pretension of lines	12,500	(kN)

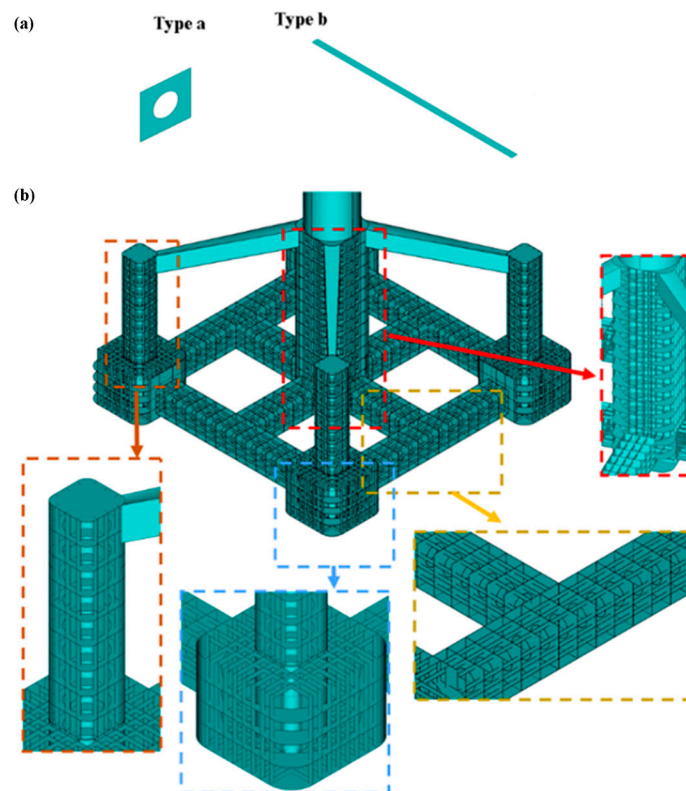


Figure 2. Designed stiffeners for the TLP; (a) stiffener types, (b) the stiffeners' arrangements inside the TLP.

Table 4. Mass details of the tower, turbine, and the platform.

Parameter	Tower	Turbine	Platform
Mass (kg)	628,442	673,998	2,208,600
Ixx (kg·m ²)	6.52 × 10 ⁸	1.66 × 10 ⁸	6.9 × 10 ⁸
Iyy (kg·m ²)	6.52 × 10 ⁸	1.06 × 10 ⁸	6.9 × 10 ⁸
Izz (kg·m ²)	7.84 × 10 ⁶	1.17 × 10 ¹⁰	1.04 × 10 ⁹
CG (m)	[0, 0, 57.5]	[0.61, 0, 131.56]	[0, 0, 8.36]

Table 5. Properties of the stiffeners.

Part	Type	Units	Thickness (m)	Height (m)	Mesh Size (m)
TLP (the hull of the structure)	-	-	0.004	-	0.50
Long Pontoon	a	13	0.016	1.00	0.50
	b	3	0.016	0.50	0.50
Short Pontoon	a	6	0.016	1.00	0.50
	b	3	0.016	0.50	0.50
Central Column	a	14	0.016	2.00	0.50
	b	4	0.016	0.80	0.50
Upper Column	a	4	0.016	0.90	0.50
	b	3	0.016	-	0.50
Lower Column	a	3	0.016	-	0.50
	b	6	0.016	1.30	0.50

2.2. Frequency Domain Diffraction/Radiation Model

Before the time-domain simulations for the moored TLP, linear diffraction and radiation calculations are conducted in ANSYS® AQWA to determine the free-floating hydrodynamic coefficients, such as added mass and damping, as well as the first-order wave exciting loads. A fixed Cartesian coordinate system is defined with the vertical z-axis pointing upwards and zero incidences of the waves when they propagate along the direction of the positive x-axis. The fluid is assumed to be inviscid and incompressible, and the flow is irrotational so that the flow can be described by velocity potentials within the domain enclosed by the boundaries defined for the problem. These include the wetted body surface, the free surface, and the sea bottom. The velocity potentials are obtained using Green’s function approach.

The submerged body surface is discretized into small panels, and a pulsating source is located on each panel. The combinations of source strengths required to diffract an incoming regular wave of a given frequency and to allow body oscillation in each degree of freedom are then calculated. Then, the incident forces, diffraction forces, added mass $a_{kj}(\omega)$, and radiation damping $b_{kj}(\omega)$ on the body are calculated. The simulations in the frequency domain for the free-floating platform were conducted for 31 frequencies. The range of frequencies is selected with care to have accurate time-domain calculations.

2.3. Time-Domain Simulation Model

The time-domain simulations are conducted using the ANSYS® AQWA time-domain module to calculate the motions and mooring load on the platform in regular waves. The equations of motion are solved at each time step, and the obtained results from the diffraction/radiation potential in the frequency domain are converted to the time domain using the retardation function approach for the hydrodynamic forces to include memory effects. According to Cummins et al. [31], the equations of motion are formulated as follows:

$$\sum_{j=1}^6 \left[\left[M_{kj} + A_{kj} \right] \ddot{x}_j(t) + \int_{-\infty}^t K_{kj}(t - \tau) \dot{x}_j(\tau) d\tau + C_{kj} \dot{x}_j(t) \right] = F_k^1(t) + F_k^m(t) \quad (1)$$

where $F_k^1(t)$ is the total first-order wave exciting forces including incident and diffraction forces. These forces can be obtained in the time domain based on the first-order wave loads obtained from the frequency domain solution. $F_k^m(t)$ are the mooring system forces for tethers, C_{kj} is the hydrostatic restoring matrix, A_{kj} is the added mass at an infinite frequency, and $K_{kj}(t)$ is the retardation function that describes the time of the generalized force k after an impulsive motion along each of the generalized coordinates j . The retardation functions $K(t)$ are the Fourier transform of the frequency-dependent damping coefficients $b_{kj}(\omega)$ obtained from the frequency domain solution as:

$$K_{kj}(t) = \frac{2}{\pi} \int_0^\infty b_{kj}(\omega) \cos(\omega t) d\omega \tag{2}$$

The frequency-independent added mass can be calculated based on the frequency-dependent added mass and retardation functions as follow:

$$A_{kj} = a_{kj} + \frac{1}{\omega} \int_0^\infty K_{kj}(t) \sin(\omega t) d\omega \tag{3}$$

While the sum frequency loads may be important for TLPs considering ringing and springing-type mooring responses, at this stage, the manuscript focuses on the TLP and considers only the first-order loads.

2.4. Mooring Simulation

Twelve mooring lines are represented in the numerical simulation with steel wires as shown in Figure 1e. The load elongation curve is defined in the numerical model according to Equation (4). the properties of the mooring lines are shown in Table 3. The applied pretension in each mooring element is tuned with the obtained pretension from the benchmark solution [7]. Before starting the time domain simulation, static equilibrium analysis is conducted to make sure that the tension leg platform starts the simulation at an equilibrium position similar to the benchmark solution.

$$Load = k_1(\delta L) \tag{4}$$

2.5. Guidelines and Standards for the TLP

In terms of analysis of offshore and floating wind turbine structures, documents such as IEC 61400-1 [32], DNV-OS-C105 [33], DNV-OS-J103 [34], DNV-OS-C101 [35], IEC 61400-3-2 [36], DNV-OS-J101 [37], and DNV-ST-0119 [38], DNV-RP-C201 [39], DNV-RP-C203 [40], and DNV-RP-C202 [41] provide some regulations and guidelines

To get some basic information about the properties of stiffeners, DNV-RP-C203 [40] and DNV-OS-C101 [35] recommendations are used. According to the DNV-OS-C101 [35], the minimum thickness should not be less than:

$$t = \frac{14.3 t_0}{\sqrt{f_{yd}}} \text{ (mm)} \tag{5}$$

where f_{yd} is design yield strength (N/mm²) and t_0 is the thickness of the structure based on the application categories of components [33]. For plates subjected to lateral pressure, the minimum thickness is determined as follows:

$$t = \frac{15.8 k_a s \sqrt{p_d}}{\sqrt{\sigma_{pd1} k_{pp}}} \text{ (mm)} \tag{6}$$

where k_a , s , p_d , σ_{pd1} , and k_{pp} are defined as a correction factor for the aspect ratio of the plate field, stiffener spacing (m), design pressure (kN/m²), design bending stress (N/mm²),

and fixation parameter for the plate, respectively. According to the DNV-OS-C101 [35], the minimum section module for stiffeners is defined as follows:

$$Z_s = \frac{l^2 s p_d}{k_m \sigma_{pd2} k_{ps}}, \text{ min } 15 \times 10^3 \text{ (mm}^3\text{)} \tag{7}$$

where l , k_m , σ_{pd2} , and k_{ps} are defined as stiffener span (m), bending moment factor, design bending stress (N/mm²), and fixation parameter for stiffeners, respectively. The minimum shear area is defined as follows (DNV-OS-C101 [35]):

$$A_s = \frac{l s p_d}{2 \tau_{pds}} 10^3 \text{ (mm}^2\text{)} \tag{8}$$

where τ_{pds} is the design shear stress (N/mm²). The height of the web is calculated as follows (DNV-RP-C202 [41]):

$$h \leq 0.4 t_w \sqrt{E / f_y} \tag{9}$$

where t_w is the thickness of the web. Therefore, based on the above formulae, the minimum thickness for stiffeners with a spacing of 1 m and a span of 2 m is 16 mm, and the minimum height of the web should be 125 mm. However, to have less stress than f_y in the structure, the web height should be 420 mm. Checks with this size of stiffeners will be conducted in the next phase of the study, dealing with the detailed structural design.

3. Development of the FEM Model

To model the TLP, Shell 281 element with eight nodes in the ANSYS is used (Figure 3). The ANSYS contact capability is utilized to model the interaction of the stiffeners and TLP. In contact between two elements, the node-to-line method is established as the target and the contact. The hull of the TLP was defined as the target surface, and the edges of the stiffeners were introduced as the contact surface. The mesh size is 0.5 m (Yeter et al. [14]) for the TLP and 1.0 m for the tower, and the turbine is 0.3 m.

The mesh size is larger in the tower as the focus is on the stress distribution on the TLP. The meshed TLP with 10 MW wind turbine and stiffeners are presented in Figure 3. To analyze the stress distribution, the rotor, and the nacelle weight are defined as a point mass, and the wind pressure is defined as a force on the top of the tower (Figure 4a). The wind force and the moment of the nacelle and the rotor are 1500 kN and 40 MN·m, respectively. The TLP is under hydrostatic pressure as the still water, as shown in Figure 4b. The TLP’s draft after installation is 20 m. Fixed boundary conditions are used in each corner of the model in the locations of tendons (Figure 4c).

To analyse the CENTEC-TLP under hydrostatic and hydrodynamic loads, after generating the model in APDL, the geometry of the model is transferred to AQWA. The simulations in the time domain are conducted on the full scale. The simulations performed in regular waves as well as the wind loads are shown in Table 6 for the above-rated conditions. The wind force and wind speed at the above-rated conditions are 800 kN and 22.4 m/s, respectively. The total simulation time is selected to be the 60 s after the transient be-haviour of the platform. The selected time step is 0.05 s. This study assumes that the TLP has mooring lines instead of steel tethers.

Table 6. The above-rated environmental conditions.

Waves		Wind (m/s)	Turbine
H (m)	T (s)		
8	11.5	22.4	Operational

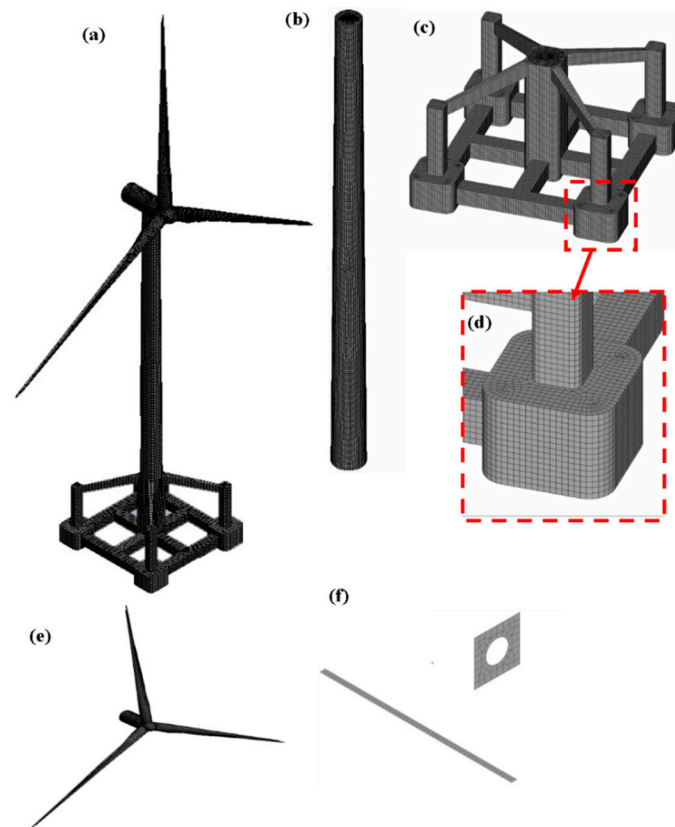


Figure 3. The meshed model of the CENTEC-TLP: (a) a perspective of the TLP with the tower and the 10 MW wind turbine; (b) the tower of the turbine; (c) the TLP; (d) the connection of the upper column with the lower column; (e) the meshed 10 MW turbine; (f) the meshed stiffeners.

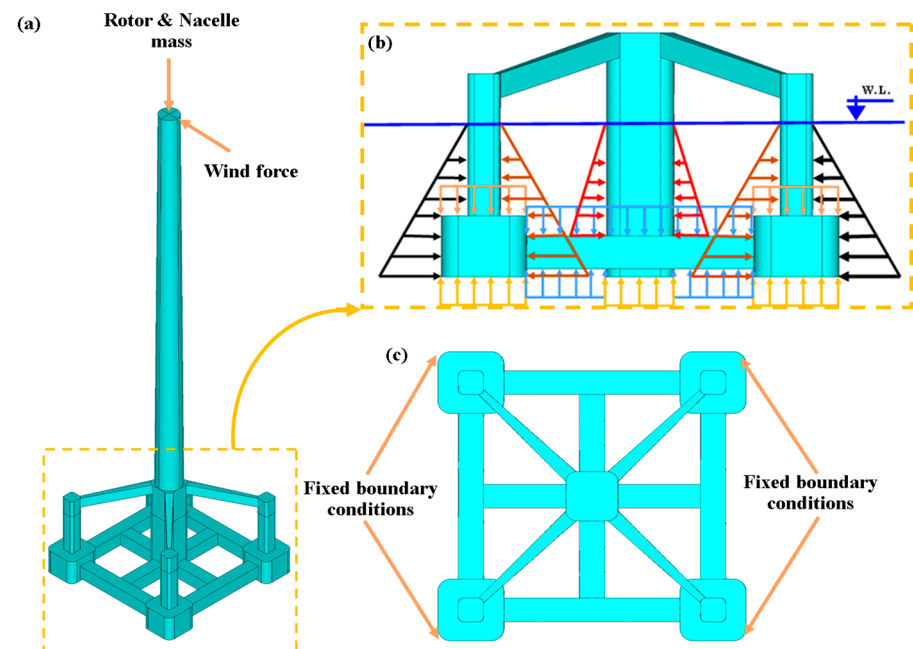


Figure 4. The loaded model: (a) location of the rotor and the nacelle mass and the wind pressure, (b) the concentrated force applied on the top of the CENTEC-TLP, (c) the locations of boundary conditions.

The benchmark values are validated by experimental models presented in [29]. Hence, to show the accuracy of the modeling, meshing, and method used, the results of the ANSYS AQWA are validated with the benchmark model.

4. Results and Discussion

In this part, the platform is first numerically analysed in the still water condition with a wind thrust applied at a constant rated wind speed. Then, hydrostatic results for the platform in both free-floating and operating conditions are validated against the benchmark solution available in the literature [7]. The study is limited to the analyses conducted in still water and above-rated conditions. At this stage, the primary objective is to investigate the highest regular waves that still have wind loads from the running turbine. In the future, the platform’s strength can be investigated under extreme loads of irregular sea states and wind coming from various directions. Due to software limitations (AQWA), the hydrodynamic analysis does not include the coupling effects between the platform and the wind turbine.

4.1. Stress Distributions on the Platform

The platform is analysed with the minimum thickness and height of stiffeners proposed by DNV-OS-C101 [35] and DNV-RP-C202 Figure 5 shows the stress distribution, and Table 7 presents the stress of the reinforced TLP.

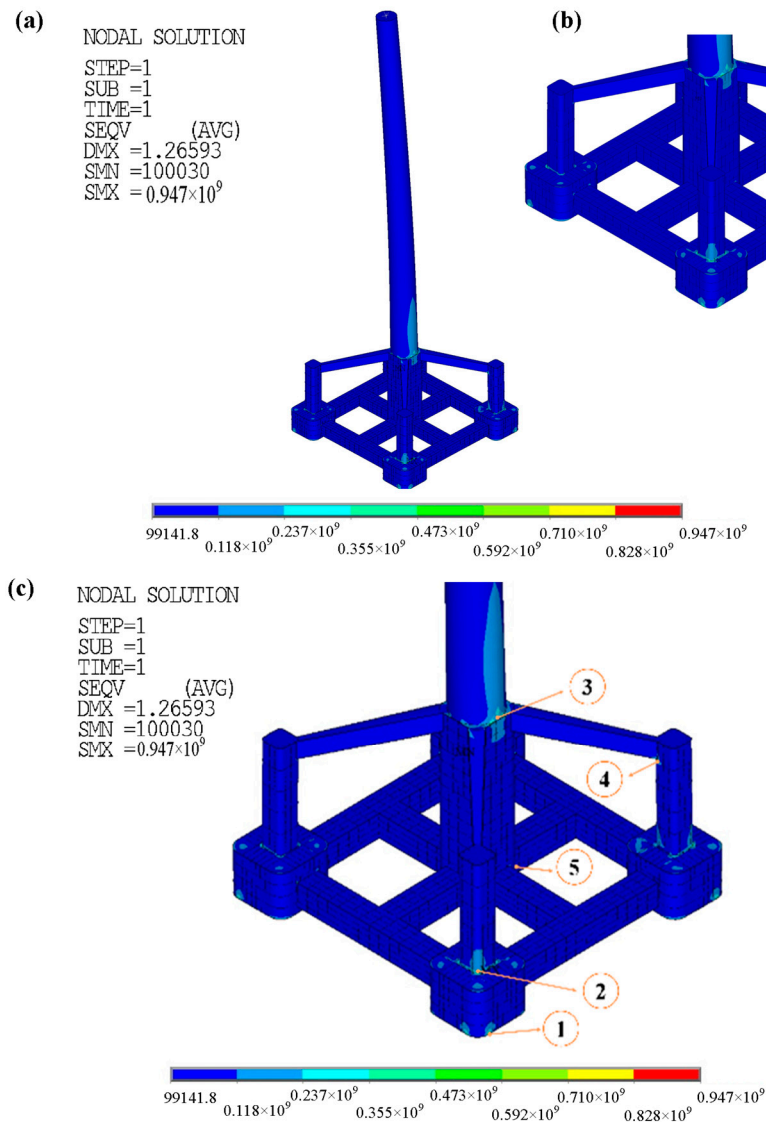


Figure 5. The stress distribution on the CENTEC-TLP with minimum stiffeners proposed by DNV-OS-C101 [35] and DNV-RP-C202 [41]; (a) the stress distribution on the TLP with tower, (b) the stress distribution on the TLP, (c) the TLP with marked maximum stresses in different points.

Table 7. The stress (MPa) in the CENTEC-TLP.

Location ¹	Von Mises Stress	X- Component of Stress	Y- Component of Stress	Z- Component of Stress	1st Principal Stress	2nd Principal Stress	3rd Principal Stress
1	601	460	498	554	659	333	0.123
2	947	541	477	537	607	300	1.39
3	762	492	545	470	550	237	5.27
4	456	490	509	459	509	387	4.78
5	681	289	465	319	506	173	0.175

¹ Locations are presented in Figure 5.

According to Figure 5 and Table 7, it can be concluded that the thickness, height, and number of stiffeners, which are determined by DNV-OS-C101 [35] and DNV-RP-C202 [41], are not enough for some parts of the TLP because the values of stress in some critical points, such as location 1, 2, and 3, are higher than the yield stress; thus, a yielding would occur in the TLP before those stress levels would be reached. As a result, these locations need to be reinforced.

These options could be stiffeners, fibre-reinforced polymer (FRP), bracket collar plates, doubler plates, or similar methods. Overall, the downwind of the TLP experienced higher stress than other parts. The increase of the thickness of the stiffeners would be one of the options to reinforce the TLP.

According to Table 8, the increase in the stiffeners’ thickness in the lower, upper, and central columns leads to a decrease in the maximum stress in different locations. It can be concluded that instead of increasing the stiffeners’ thickness in the mentioned three parts to 40 mm, it is better to increase the thickness of the stiffeners in the lower column to 40 mm, in the upper column to 30 mm, and in the central column to 35. Table 8 presents the effects of the combination of different thicknesses on the stress in the CENTEC-TLP.

Table 8. The effects of the stiffeners’ thickness of the lower, the upper, and the central column on stress in the CENTEC-TLP.

Location ¹	Stress (MPa)				
	20 mm	25 mm	30 mm	35 mm	40 mm
1	576	567	560	555	550
2	924	778	676	599	539
3	673	595	528	474	429
4	429	419	413	406	401
5	561	467	402	354	317

¹ Locations are presented in Figure 5.

The results indicate that increasing the thickness of all stiffeners compared with the increase of the thickness of the lower, upper, and central columns has negligible effects on the maximum stresses of different locations. Thus, the thickness of the lower, upper, and central columns just increased. Table 9 presents the effects of the stiffeners’ thickness on stress in the TLP.

Table 9. The stress (MPa) in the CENTEC-TLP by increased thicknesses.

Location ¹	Von Mises Stress	X- Component of Stress	Y- Component of Stress	Z- Component of Stress	1st Principal Stress	2nd Principal Stress	3rd Principal Stress
1	563	429	451	434	611	307	1.6
2	412	417	423	415	475	253	1.33
3	474	463	351	276	467	199	4.44
4	413	523	502	487	533	375	4.61
5	354	234	309	225	309	136	0.172

¹ Locations are presented in Figure 5.

The values are calculated in the current loading condition and the safety factor(s) need to be applied in WSD/LRFD approaches. In the following subsections, the stress distribution in each part of the TLP will be discussed.

4.1.1. The Pontoons

The stress distribution on the pontoons in the TLP is presented in Figure 6. According to Figure 6d,f the pontoons connected to the central column downwind of the TLP have more stress than other parts of the pontoons. It can be seen that the bottom of the pontoons, especially pontoons that are in the leeward of the TLP, have more stress because of having both the hydrostatic pressure and the wind force together; therefore, that part should be reinforced by appropriate methods (Figure 6f).

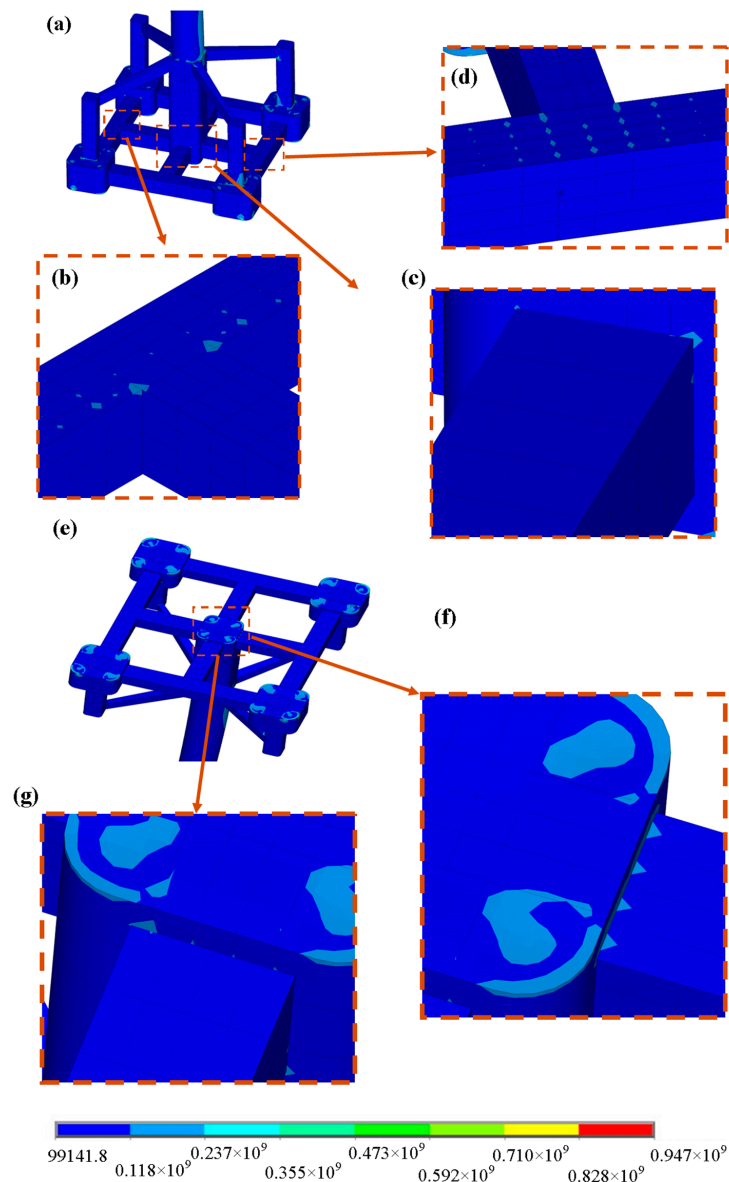


Figure 6. The stress distribution on the pontoons in the CENTEC-TLP; (a) a close view of the TLP, (b) the stress distribution on the pontoons on the opposite side of the TLP, (c) the stress distribution on the connection of pontoons with the central column, (d) the stress distribution on the downwind parts of the pontoon, (e) the stress distribution on the bottom of the TLP, (f) the stress distribution on the downwind parts of the pontoon in the bottom, (g) the stress distribution on the connection of the pontoon with the central column at the bottom.

4.1.2. The Lower Column and the Mooring Connections

The stress distribution on the lower column and the mooring connections in the TLP is presented in Figure 7. It can be seen that stress concentration appears in the mooring connections and the interaction of the lower column with the upper column, especially the corners that are close to the mooring lines. Figure 7d indicates that the inside parts of the lower column get less stress than the outside parts. All corners of the lower columns and the mooring connections need extra support by stiffeners or other reinforcing methods.

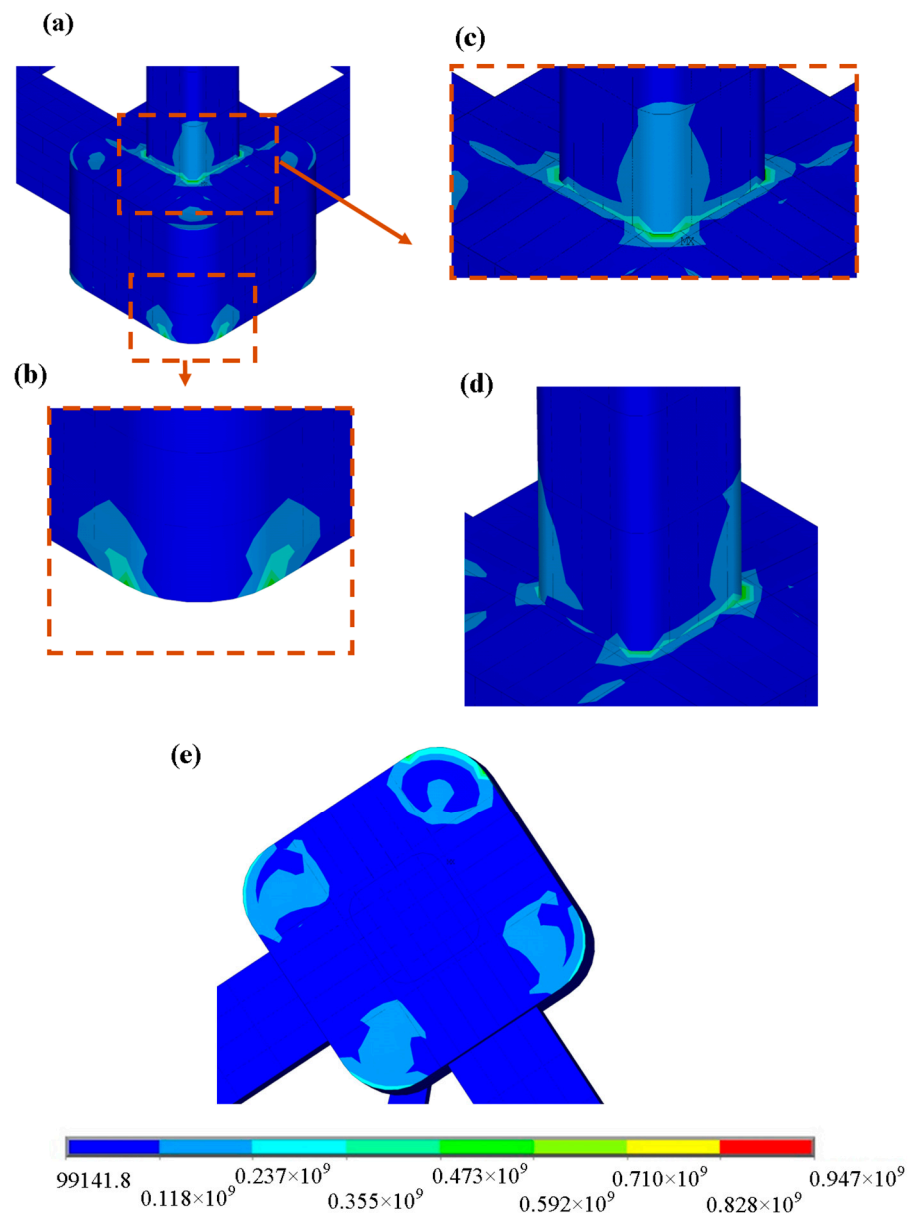


Figure 7. The stress distribution on the lower column and the mooring connections in the CENTEC-TLP; (a) a close view of the lower column, (b) the stress distribution on the mooring connections, (c) the stress distribution on the interaction of the lower column with the upper column (outside), (d) the stress distribution on the interaction of the lower column with the upper column (inner side), (e) the stress distribution on the bottom of the lower column.

4.1.3. The Central Column

Figure 8 indicates the connection between the tower of the DTU 10 MW and the central column. According to Figure 8c, the interaction of the tower with the central column and the bottom of the central column, all corners of the TLP should be reinforced.

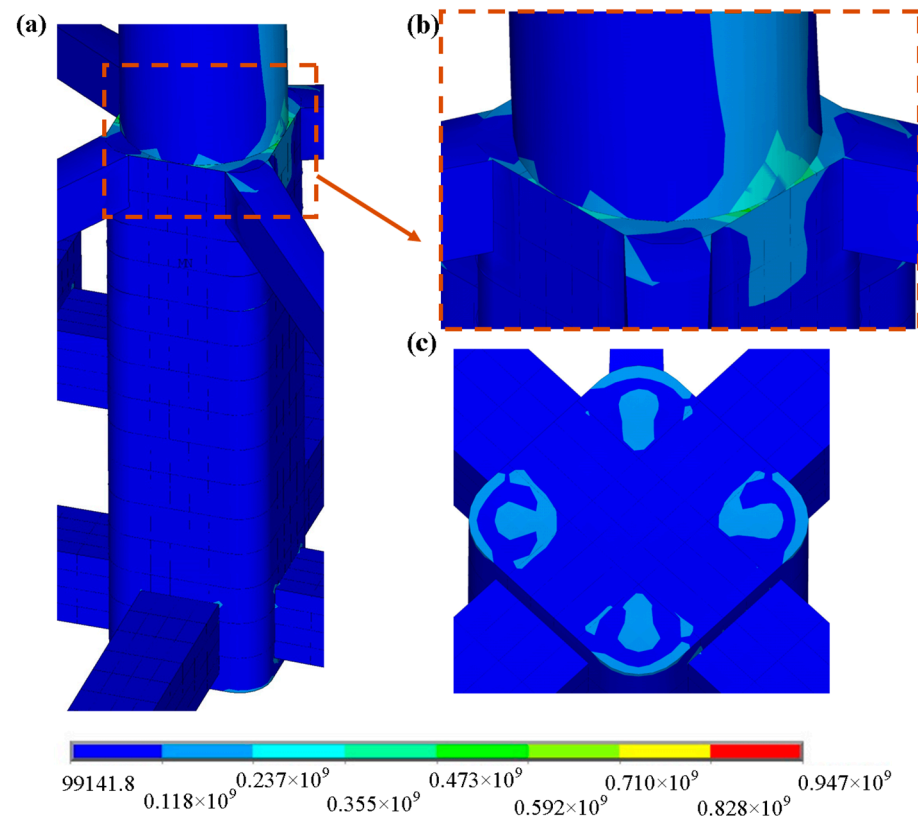


Figure 8. The stress distribution on the central column in the CENTEC-TLP; (a) a close view of the central column, (b) the stress distribution on the connection of the tower of the DTU 10 MW and central column, (c) the stress distribution on the bottom of the central column.

4.1.4. The Upper Column and the Support Brace

The stress distribution on the upper column and the support brace in the TLP is pre-sented in this section. Figure 9 shows that stress concentration could be seen in the inter-action of the lower column and support brace with the upper column on the leeward side of the TLP. According to Figure 9c, the bottom of the support brace requires more stiffener than the top of the support brace. Figure 9d indicates that other support braces which are not in downwind of the TLP have less stress concentration.

4.2. Hydrodynamic Response of the CENTEC-TLP

4.2.1. The Free-Floating Condition

The platform is designed to be assembled as a system with the platform, tower, and turbine at the shoreline. It can be transported in this condition with a draft of 3.85 m. AQWA calculates the metacentric height in the free-floating case as 26.41 m, which presents a 5% difference from the benchmark's metacentric height. This is because of some of the volumetric differences caused by mesh size differences and the mooring line modelling. By looking closely at Table 10, it can be seen that the results of the AQWA are similar to the results of the benchmark case. Therefore, the modelling, meshing size, and mass distribution are considered acceptable. The TLP validated experimentally is available in [29]. Figure 10 depicts the response amplitude operators of the platform's motions in the free-floating condition. The platform is transported in Galicia, Spain, where the majority of small waves have periods between 5 and 10 s, as shown in [7]. The results indicate that the platform's greatest pitch RAO between these wave periods is $0.38^\circ/\text{m}$, while the largest heave RAO is less than 1.4.

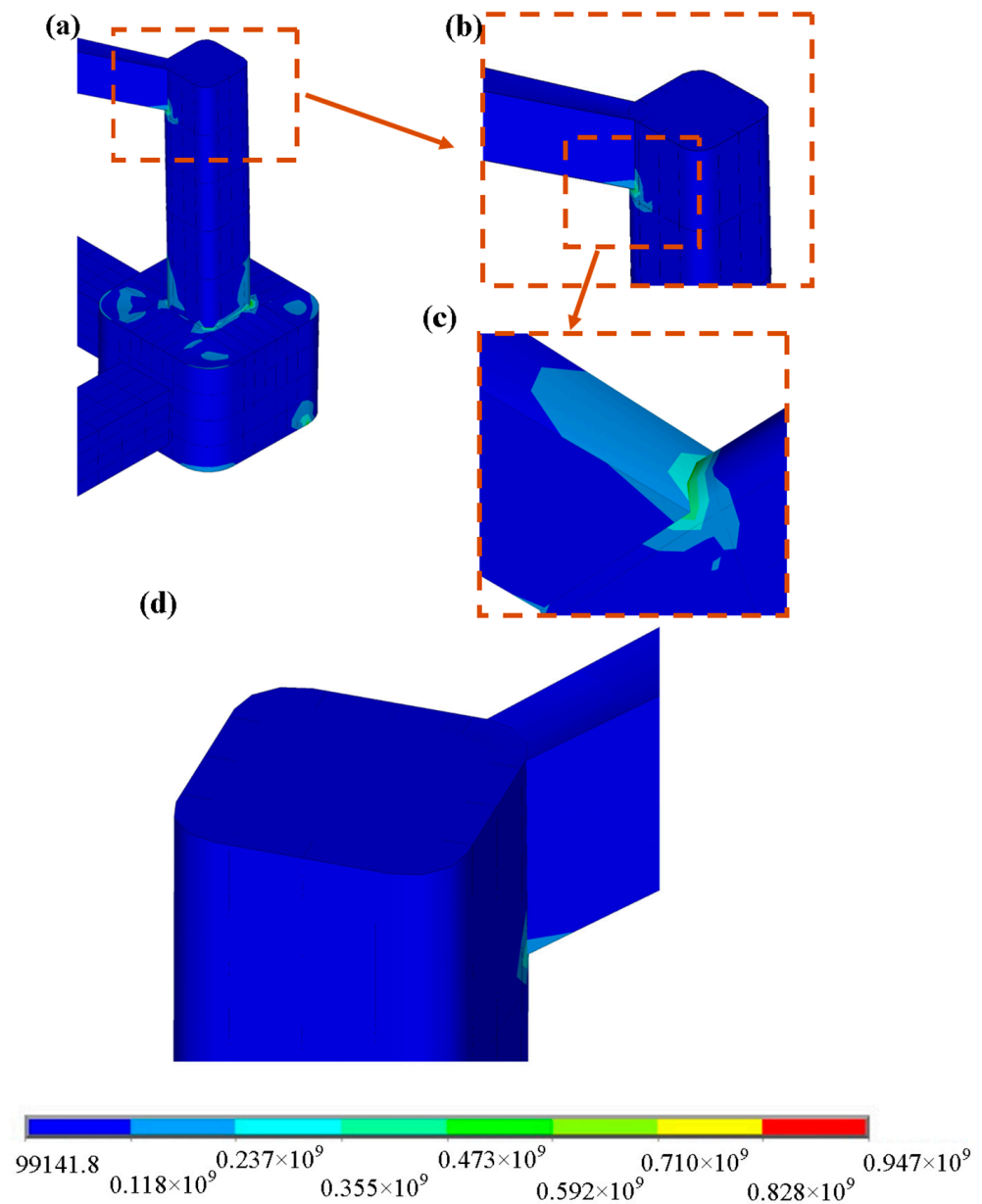


Figure 9. The stress distribution on the upper column and the support brace in the CENTEC-TLP; (a) a close view of the upper column, (b) the stress distribution on the connection of the support brace and upper column in the leeward, (c) the stress distribution on the bottom of support brace in the leeward, (d) the stress distribution on the bottom of support brace.

Table 10. Comparison of the characteristics of obtained in AQWA and Benchmark (BM) model in transport condition.

Parameter	BM	AQWA	Error %
Transport condition GM (m)	27.76	26.41	−5%
Transport draft (m)	3.85	3.85	0%
Displacement (ton)	3511	3511	0%
Static pitching angle (deg)	0.22	0.20	−9%
Heave natural period (s)	4.7	4.50	−4%
Roll and Pitch natural period (s)	22.3	24.38	9%

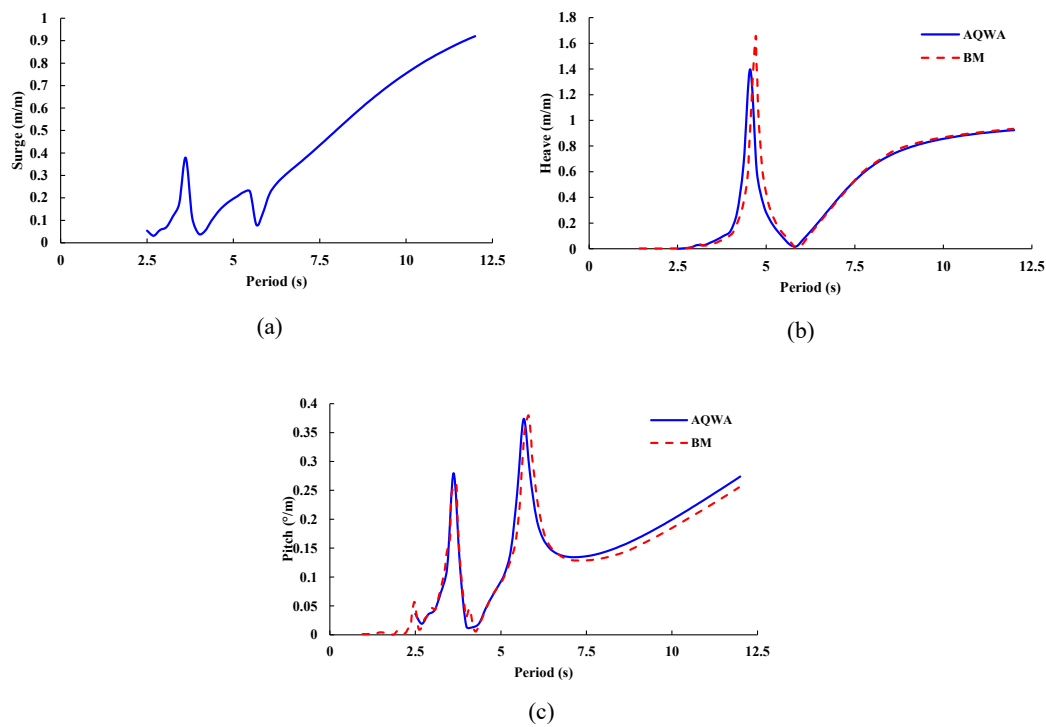


Figure 10. Response amplitude operator of the platform in its free-floating condition: (a) surge; (b) heave; (c) pitch.

4.2.2. Natural Frequencies in the Installed Condition

The platform is installed with 12 mooring lines at a 20-m draft. The characteristics of the platform in the installation position are shown in Table 10. The natural frequency of the benchmark model with the AQWA model is compared, and the results are provided in Table 11. Thus, it is concluded that, for this environmental setup, AQWA and the Benchmark results are in good agreement. The leading cause of the difference is modelling mooring lines as steel tethers.

Table 11. Comparison between the natural frequency obtained by AQWA and the benchmark (BM) model.

Parameter	Units	Surge	Pitch	Heave
BM	Hz	0.029	0.207	0.481
AQWA		0.030	0.280	0.500
BM	s	35.71	4.83	2.08
AQWA		33	4	2

4.2.3. The Above-Rated Operation Condition

The results of the isolated steady wind and regular wave loads are provided in this section. The data are provided for a single wave direction (head wave). The values of the wave and wind in the above-rated conditions are presented in Table 6. Figure 11 presents the time series of motions and Figure 12 mooring forces obtained in regular waves. Results of isolated steady wind and regular waves in the above-rated conditions are shown in Tables 12 and 13, respectively. The obtained results show that the difference in the surge motion is 5 to 7% and 10 to 20% in heave motion. In the pitch rotation, the difference is about 14 to 16%, and the maximum difference in the mooring lines is 9 to 19%. Under steady wind loads, the difference is about 0 to 2%. The differences in the isolated case are not too high. Thus, it can be concluded that there is a good agreement between the AQWA and the benchmark model.

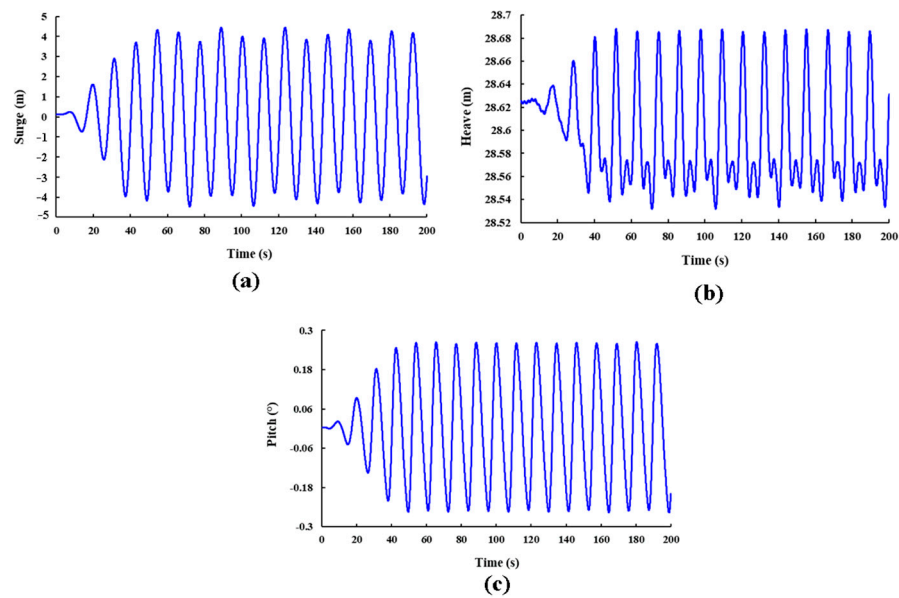


Figure 11. The time series of motions obtained in the regular wave: (a) surge (m); (b) heave (m); (c) pitch (degree).

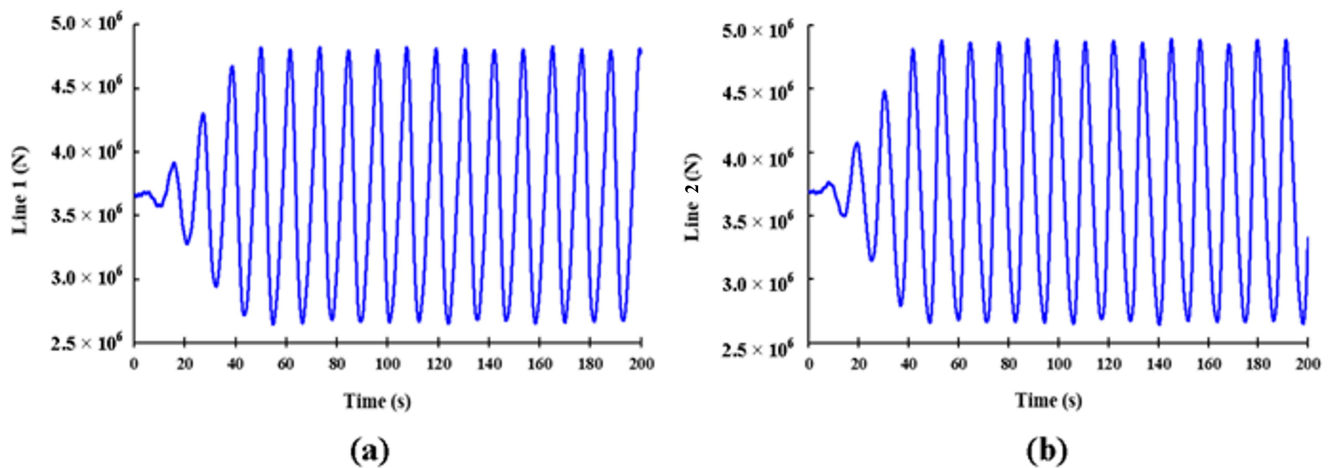


Figure 12. The mooring forces obtained in the regular wave. (a) Line 1; (b) Line 2.

Table 12. Platform responses to the regular waves in above-rated conditions.

Parameter		Benchmark (BM)	AQWA	Error %
Isolated Motions Type		Wave	Wave	
Surge (m)	min	−3.89	−4.16	−7%
	max	4.1	4.32	−5%
Heave (m)	min	−0.1	−0.09	10%
	max	0.05	0.06	−20%
Pitch (deg)	min	−0.29	−0.25	14%
	max	0.31	0.26	16%
Line 1 (kN)	min	2219	2640	−19%
	max	5058	4822	5%
Line 2 (kN)	min	2430	2656	−9%
	max	4894	4876	0%

Table 13. Results of the platform in the above-rated conditions at a steady wind.

Isolated Motions Type	Benchmark (BM)	AQWA	%
	Wind	Wind	
Surge (m)	1.93	1.9	2%
Heave (m)	0	0	0%
Pitch (deg)	0.09	0.09	0%
Line 1 (kN)	3339	3392	−2%
Line 2 (kN)	3993	4069	−2%

5. Conclusions

The stress distribution on the CENTEC-TLP at the design condition in still water and the response of the platform is determined in the time domain under wave and wind load conditions. The main conclusions are summarized as follows:

- pontoons downwind of the TLP have high stress in the connection of the pontoons with the central column and lower columns.
- The stress concentration is seen in the interaction of the lower column and the support brace with the upper column on the leeward side of the TLP. The lower column, especially the corners close to the mooring lines, has higher stress values than other corners of the lower column. The mooring connections show high stress. Therefore, they should be reinforced with methods, such as an increased thickness of the stiffeners, number of stiffeners, or others.
- Overall, the leeward of the TLP needs more attention and precise design because that side had higher stress values.
- In the free-floating condition, the maximum difference between the benchmark results and the AQWA in GM is 5%.
- In natural frequencies, a difference of 8% in the roll and pitch, and 4% in the heave was shown.
- The mean difference between the results of the isolated wave of benchmark and AQWA model in surge, heave, and pitch is −7%, 20%, and 16%, respectively.
- The maximum mooring force of the isolated wave of the benchmark and AQWA model in line 1 is 4874, and in line 2 is 4893, which signifies a 4 and 0% difference.
- The differences of 2%, 0%, and 0% in the surge, heave, and pitch in the isolated wind are shown between the results of the benchmark and the AQWA model.
- The mooring line forces of the isolated wind of the benchmark and AQWA model in line 1 is 3392, and in line 2 is 4069, which signifies a −2% difference in both cases.
- This study focused on the above-rated condition which is a combination of wind and wave loading. Investigating the TLP against extreme loads and multivariate statistical methods or time-frequency domain analysis can be an important topic for future studies.

Author Contributions: Conceptualization, C.G.S., E.U. and B.-Q.C.; methodology, E.Z. and H.S.A.; formal analysis, E.Z. and H.S.A.; visualization, E.Z. writing—original draft preparation, E.Z. and H.S.A.; writing—review and editing, E.U., B.-Q.C. and C.G.S.; Supervision C.G.S. All authors have read and agreed to the published version of the manuscript.

Funding: This work was performed within the project ARCWIND—Adaptation and implementation of floating wind energy conversion technology for the Atlantic region, which is co-financed by the European Regional Development Fund through the Interreg Atlantic Area Programme under contract EAPA 344/2016. This work contributes scope of the Strategic Research Plan of the Centre for Marine Technology and Ocean Engineering (CENTEC), which is financed by the Portuguese Foundation for Science and Technology (Fundação para a Ciência e Tecnologia—FCT) under contract UIDB/UIDP/00134/2020. The second author is funded by FCT with a PhD grant under contract 2020.06969.BD.

Institutional Review Board Statement: Not applicable.

Informed Consent Statement: Not applicable.

Data Availability Statement: Not applicable.

Acknowledgments: Already under Funding.

Conflicts of Interest: The authors declare no conflict of interest.

References

1. Díaz, H.; Serna, J.; Nieto, J.; Guedes Soares, C. Market Needs, Opportunities and Barriers for the Floating Wind Industry. *J. Mar. Sci. Eng.* **2022**, *10*, 934. [[CrossRef](#)]
2. Díaz, H.; Guedes Soares, C. Review of the current status, technology and future trends of offshore wind farms. *Ocean Eng.* **2020**, *209*, 107381. [[CrossRef](#)]
3. Díaz, H.; Teixeira, A.; Guedes Soares, C. Application of Monte Carlo and Fuzzy Analytic Hierarchy Processes for ranking floating wind farm locations. *Ocean Eng.* **2022**, *245*, 110453. [[CrossRef](#)]
4. Bagbanci, H.; Karmakar, D.; Guedes Soares, C. Review of offshore floating wind turbines concepts. In *Maritime Engineering and Technology*; Guedes Soares, C., Garbatov, Y., Sutulo, S., Santos, T.A., Eds.; Taylor & Francis Group: London, UK, 2012; pp. 567–576. [[CrossRef](#)]
5. Leroy, V.; Delacroix, S.; Merrien, A.; Bachynski-Polić, E.; Gilloteaux, J.-C. Experimental investigation of the hydroelastic response of a spar-type floating offshore wind turbine. *Ocean Eng.* **2022**, *255*, 111430. [[CrossRef](#)]
6. Bagbanci, H.; Karmakar, D.; Guedes Soares, C. Comparison of Spar and Semisubmersible Floater Concepts of Offshore Wind Turbines Using Long-Term Analysis. *J. Offshore Mech. Arct. Eng.* **2015**, *137*, 061601. [[CrossRef](#)]
7. Uzunoglu, E.; Guedes Soares, C. Hydrodynamic design of a free-float capable tension leg platform for a 10 MW wind turbine. *Ocean Eng.* **2020**, *197*, 106888. [[CrossRef](#)]
8. Vijay, K.; Karmakar, D.; Uzunoglu, E.; Guedes Soares, C. Performance of barge-type floaters for floating wind turbine. In *Progress in Renewable Energies Offshore*; Guedes Soares, C., Ed.; Taylor & Francis Group: London, UK, 2016; pp. 637–645. [[CrossRef](#)]
9. Bak, C.; Zahle, F.; Bitsche, R.; Kim, T.; Yde, A.; Henriksen, L.C.; Hansen, M.H.; Blasques, J.P.A.A.; Gaunaa, M.; Natarajan, A. *The DTU 10-MW Reference Wind Turbine*; DTU Wind Energy, Technical University of Denmark: Lyngby, Denmark, 2013.
10. Reyno, H.; Park, J.-S.; Kang, S.-Y.; Kang, Y.-J. A Numerical Analysis for Stress Concentration of Openings in Offshore Tubular Steel Tower under Design Loading Condition. *J. Korea Acad. Coop. Soc.* **2015**, *16*, 1516–1523. [[CrossRef](#)]
11. Akbas, U.B.; Shen, J. Design issues of wind turbine towers. In Proceedings of the 8th International Conference on Structural Dynamics, Leuven, Belgium, 4–6 July 2011; pp. 1592–1598.
12. Yeter, B.; Garbatov, Y.; Guedes Soares, C. Fatigue damage assessment of fixed offshore wind turbine tripod support structures. *Eng. Struct.* **2015**, *101*, 518–528. [[CrossRef](#)]
13. Yeter, B.; Garbatov, Y.; Guedes Soares, C. Structural design of an adaptable jacket offshore wind turbine support structure for deeper waters. In *Maritime Technology and Engineering 3*; Guedes Soares, C., Santos, T.A., Eds.; Taylor & Francis Group: London, UK, 2016; pp. 583–594. [[CrossRef](#)]
14. Teixeira, R.; Noyal, M.; O’connor, A.; Nichols, J.; Dumas, A. Stress-cycle fatigue design with Kriging applied to offshore wind turbines. *Int. J. Fatigue* **2019**, *125*, 454–467. [[CrossRef](#)]
15. Kim, H.J.; Jang, B.S.; Park, C.K.; Bae, Y.H. Fatigue analysis of floating wind turbine support structure applying modified stress transfer function by artificial neural network. *Ocean Eng.* **2018**, *149*, 113–126. [[CrossRef](#)]
16. Bachynski, E.E.; Moan, T. Design considerations for tension leg platform wind turbines. *Mar. Struct.* **2012**, *29*, 89–114. [[CrossRef](#)]
17. Oguz, E.; Clelland, D.; Day, A.H.; Incecik, A.; López, J.A.; Sánchez, G.; Almeria, G.G. Experimental and numerical analysis of a TLP floating offshore wind turbine. *Ocean Eng.* **2018**, *147*, 591–605. [[CrossRef](#)]
18. Sclavounos, P.; Tracy, C.; Lee, S. Floating Offshore Wind Turbines: Responses in a Seastate Pareto Optimal Designs and Economic Assessment. In Proceedings of the International Conference on Offshore Mechanics and Arctic Engineering 2008, Estoril, Portugal, 15–20 June 2008; Paper OMAE2008-48234. pp. 31–41. [[CrossRef](#)]
19. Nematbakhsh, A.; Bachynski, E.E.; Gao, Z.; Moan, T. Comparison of wave load effects on a TLP wind turbine by using computational fluid dynamics and potential flow theory approaches. *Appl. Ocean Res.* **2015**, *53*, 142–154. [[CrossRef](#)]
20. Jamalkia, A.; Etefagh, M.M.; Mojtahedi, A. Damage detection of TLP and Spar floating wind turbine using dynamic response of the structure. *Ocean Eng.* **2016**, *125*, 191–202. [[CrossRef](#)]
21. Mas-Soler, J.; Uzunoglu, E.; Bulian, G.; Guedes Soares, C.; Souto-Iglesias, A. An experimental study on transporting a free-float capable tension leg platform for a 10 MW wind turbine in waves. *Renew. Energy* **2021**, *179*, 2158–2173. [[CrossRef](#)]
22. Sreebhadra, M.; Rony, J.; Karmakar, D.; Guedes Soares, C. Extreme response analysis for TLP-type floating wind turbine using Environmental Contour Method. In *Trends in Maritime Technology and Engineering*; Guedes Soares, C., Santos, T.A., Eds.; Taylor and Francis: London, UK, 2022; pp. 315–324. [[CrossRef](#)]
23. Guo, X.; Zhang, Y.; Yan, J.; Zhou, Y.; Yan, S.; Shi, W.; Li, X. Integrated Dynamics Response Analysis for IEA 10-MW Spar Floating Offshore Wind Turbine. *J. Mar. Sci. Eng.* **2022**, *10*, 542. [[CrossRef](#)]
24. Diaz, H.M.; Silva, D.; Bernardo, C.; Guedes Soares, C. Micro siting of floating wind turbines in a wind farm using a multiple-criteria framework. *Renew. Energy* **2023**, *204*, 449–474. [[CrossRef](#)]

25. Salvação, N.; Guedes Soares, C. Wind resource assessment offshore the Atlantic Iberian coast with the WRF model. *Energy* **2017**, *145*, 276–287. [[CrossRef](#)]
26. Silva, D.; Bento, A.R.; Martinho, P.; Guedes Soares, C. High resolution local wave energy modelling in the Iberian Peninsula. *Energy* **2015**, *91*, 1099–1112. [[CrossRef](#)]
27. Costa, T.C.; Pereira, L.T.; Marta-Almeida, M.; Guedes Soares, C. Mapping of currents off the northwestern Iberian coast with the Regional Ocean Modelling System. *J. Oper. Oceanogr.* **2018**, *13*, 71–83. [[CrossRef](#)]
28. Uzunoglu, E.; Guedes Soares, C. Parametric modelling of marine structures for hydrodynamic calculations. *Ocean Eng.* **2018**, *160*, 181–196. [[CrossRef](#)]
29. Hmedi, M.; Uzunoglu, E.; Medina-Manuel, A.; Mas-Soler, J.; Vittori, F.; Pires, O.; Azcona, J.; Souto-Iglesias, A.; Guedes Soares, C. Experimental Analysis of CENTEC-TLP Self-Stable Platform with a 10 MW Turbine. *J. Mar. Sci. Eng.* **2022**, *10*, 1910. [[CrossRef](#)]
30. Chakrabarti, S. *Handbook of Offshore Engineering*; 2-Volume Set; Elsevier: Oxford, UK, 2005.
31. Cummins, W.E. The impulse response function and ship motions. *Schiffstechnik* **1962**, *9*, 101–109.
32. IEC 61400-1; Wind Turbines—Part 1: Design Requirements. International Electrotechnical Commission: Geneva, Switzerland, 2005; No. 2, p. 88. Available online: <https://webstore.iec.ch/publication/26423> (accessed on 12 April 2023).
33. DNVGL-OS-C105; Structural Design of TLPS (LRFD Method). Det Norske Veritas: Høvik, Norway, 2011; Volume DNV-OS-C10, p. 38. Available online: <https://rules.dnv.com/servicedocuments/dnvpmp/> (accessed on 12 April 2023).
34. DNV-OS-J103; Design of Floating Wind Turbine Structures. Det Norske Veritas: Høvik, Norway, 2013. Available online: <https://rules.dnv.com/servicedocuments/dnvpmp/> (accessed on 12 April 2023).
35. DNV-OS-C101; Design of Offshore Steel Structures, General (LRFD Method). Det Norske Veritas: Høvik, Norway, 2011; p. 2015. Available online: <https://rules.dnv.com/servicedocuments/dnvpmp/> (accessed on 12 April 2023).
36. IEC 61400-3-2; Design Requirements for Floating Offshore Wind Turbines. International Electrotechnical Commission: Geneva, Switzerland, 2020. Available online: <https://webstore.iec.ch/publication/29244> (accessed on 12 April 2023).
37. DNV-OS-J101; Design of Offshore Wind Turbine Structures. Det Norske Veritas: Høvik, Norway, 2014; pp. 212–214. Available online: <https://rules.dnv.com/servicedocuments/dnvpmp/> (accessed on 12 April 2023).
38. DNVGL-ST-0119; DNV GL Standard for Floating Wind Turbines. Det Norske Veritas: Høvik, Norway, 2018. [[CrossRef](#)]
39. DNV-RP-C201; Buckling Strength of Plated Structures. Det Norske Veritas: Høvik, Norway, 2002. [[CrossRef](#)]
40. DNVGL-RP-C203; Fatigue Design of Offshore Structures. Det Norske Veritas: Oslo, Norway, 2016. [[CrossRef](#)]
41. DNV-RP-C202; Buckling Strength of Shells. Det Norske Veritas: Høvik, Norway, 2013; p. 27. [[CrossRef](#)]

Disclaimer/Publisher’s Note: The statements, opinions and data contained in all publications are solely those of the individual author(s) and contributor(s) and not of MDPI and/or the editor(s). MDPI and/or the editor(s) disclaim responsibility for any injury to people or property resulting from any ideas, methods, instructions or products referred to in the content.